J Mater Sci: Mater Electron **(2023) 34:2230**

Energy transfer and optical properties of $NaLaMgWO_6$:Dy^{3+}, Tb^{3+} phosphors

Zhe Wang[1], Shihui Zhou[1], Pu Hu[1], Zhiliang Huang[1], and Zhanhui Zhang[1,*]

[1] *School of Materials Science and Engineering & Hubei Key Laboratory of Plasma Chemistry and Advanced Materials, Wuhan Institute of Technology, Wuhan 430205, China*

Received: 17 July 2023
Accepted: 31 October 2023
Published online: 30 November 2023

ABSTRACT

In this study, we have prepared several $NaLaMgWO_6$:Dy^{3+}, Tb^{3+} phosphors using a high-temperature solid-phase method. X-ray diffraction (XRD) and photoluminescence (PL) were used to analyze the physical phase and luminescent characteristics of these materials. Our results showed that in the $NaLaMgWO_6$:xDy^{3+} phosphor, an ideal doping concentration of $x = 8.0$ mol% was discovered, which gave off a noticeably yellowish emission band. In $NaLaMgWO_6$:yTb^{3+} phosphor, the optimal doping concentration of Tb^{3+} ions were $y = 10$ mol%. Dy^{3+} and Tb^{3+} singly doped phosphors showed significant yellow and green emission at 574 nm and 547 nm, corresponding to the $^4F_{9/2} \rightarrow {}^6H_{13/2}$ transitions of Dy^{3+} and the $^5D_4 \rightarrow {}^7F_5$ transitions of Tb^{3+}, respectively. In the $NaLaMgWO_6$:Dy^{3+}, Tb^{3+} phosphor, energy transfer was observed, and the mechanism behind it was thoroughly described. Furthermore, the color of the $NaLaMgWO_6$ phosphor could be adjusted from yellowish to greenish by varying the Dy^{3+}/Tb^{3+} ratio in concentration. These findings demonstrate that co-doped $NaLaMgWO_6$ phosphors containing $Dy^{3+}$and Tb^{3+} hold great potential for use in gadgets with fluorescent displays.

1 Introduction

White light-emitting diodes (w-LEDs) with phosphor conversion have become a very popular source of solid-state illumination in the past few years. This is due to their remarkable characteristics such as excellent luminance output, a long lifespan, minimal energy use, and environmental sustainability [1]. At present, commercial w-LEDs create light principally by combining blue-emitting InGaN chips with yellow-emitting phosphorescent (YAG: Ce^{3+}). However, low color rendering index (CRI) and correlated color temperature (CCT) are caused by the absence of a red component in the visible zone, which makes LED devices less than optimal for display purposes. Therefore, it is crucial and necessary to investigate the regulation of phosphors and phosphors' chromaticity coordinates for different color emission [2–5].

Phosphors utilize rare earth ions as luminescent centers because of their distinctive electronic structure and rich luminescence hues. Two general pathways for rare earth ion activation of phosphors exist: (1) broadband emission stemming from internal d-f transitions, and (2) the generation of narrowband emission through internal f-f transitions [6–10]. Dy^{3+} ions are often used as activators for doping in phosphors due

Address correspondence to E-mail: zzhlzu@163.com

to their low price, high quantum efficiency, and good thermal stability. Green luminescent materials typically benefit from the activation of Tb^{3+} ions, which is attributed to its $^5D_4 \rightarrow {}^7F_5$ transition. Generally speaking, the doping of rare earth ions can cause different colors of luminescence, and its CIE color coordinates will also change differently. Therefore, the CIE color coordinates can be used to observe whether multiple rare earth doped luminescent materials can achieve tunable emission [11, 12]. The transition of Dy^{3+} enables it to absorb n-UV light at 364 nm and 386 nm, While in many substrates the excitation spectra of Tb^{3+} and the emission spectrum of Dy^{3+} overlap. Due to this overlap, energy may be transferred from Dy^{3+} to Tb^{3+}, creating a flexible green emission strategy [13–17].

Rare earth ions' (Dy^{3+} and Tb^{3+}) luminescence properties commonly rely on the host material's crystal structure. To achieve an efficient phosphor, it's crucial to opt for a suitable host material [18, 19]. Lately, study on double perovskite compounds with the general formula AA'BB'O_6 has been extensive. These compounds include various activators and host elements. This is because they possess superb luminescent, chemical, and physical properties. The diversity of crystal structures in AA'BB'O_6 compounds occurs due to variations in A/A' and B/B' ion types [20–26]. One of the compounds that stands out is $NaLaMgWO_6$ (NLMWO). This chemical has a monoclinic structure with a double-ordered configuration and a C2/m space group. This arrangement includes alternating layered A-site cation ordering of Na^+ and La^{3+}, and alternating

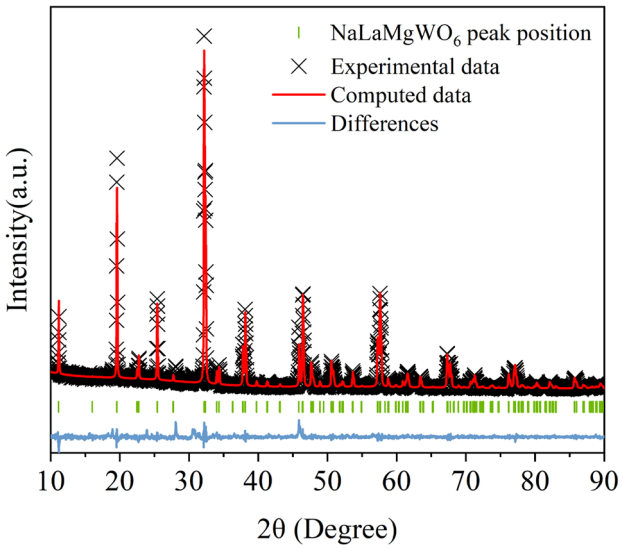

Fig. 2 Rietveld refinement pattern of NaLa0.84MgWO6: $0.08Dy^{3+}$, $0.08Tb^{3+}$

rock-salt B-site cation ordering of Mg^{2+} and W^{6+}. This arrangement generates a sizable crystal field that enables extensive co-doping of rare earth ions. The doping enables fine-tuning of the luminescent properties to achieve desirable effects. In addition, the ultraviolet region of the NLMWO matrix displays a wide and robust charge transfer band. It effectively transfers its energy to the rare earth activator, resulting in an increase in luminescence efficiency [27]. Consequently, research on rare earth ion-doped NLMWO phosphors has been considerable, especially Dy^{3+} mono-doped

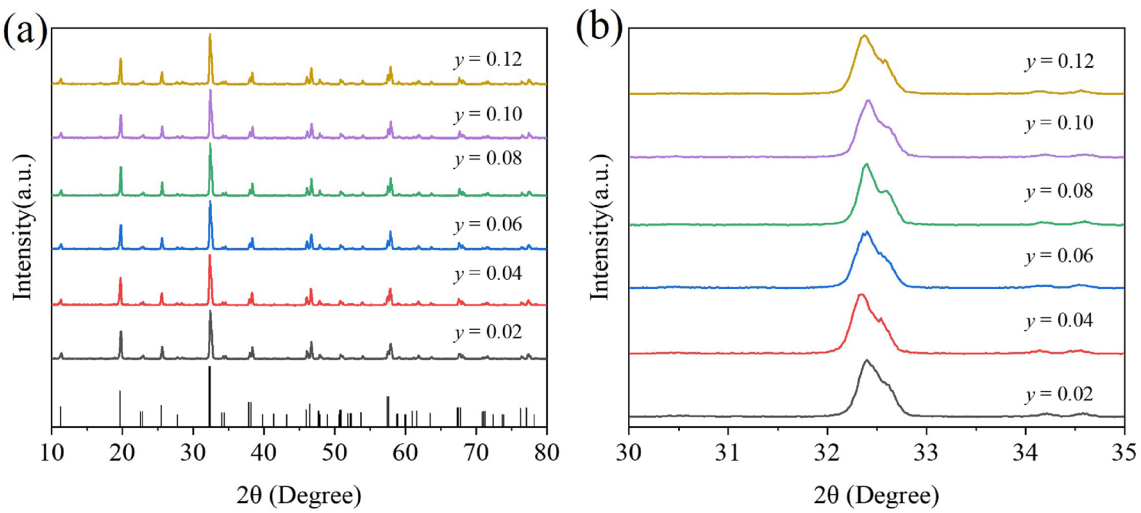

Fig. 1 **a** XRD patterns and **b** amplified XRD patterns of NaLa0.92-yMgWO6:$0.08Dy^{3+}$, yTb^{3+} phosphors

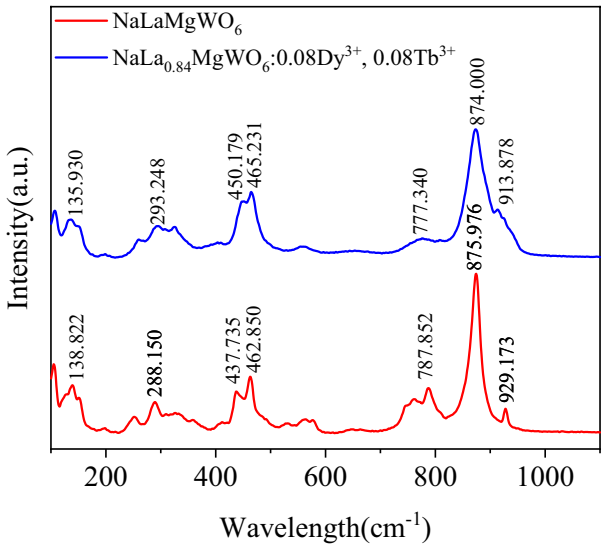

Fig. 3 Raman spectra of NLMWO and NaLa0.84MgWO6:0.08 Dy^{3+}, 0.08Tb^{3+} phosphors in the range of 100–1200 cm^{-1}

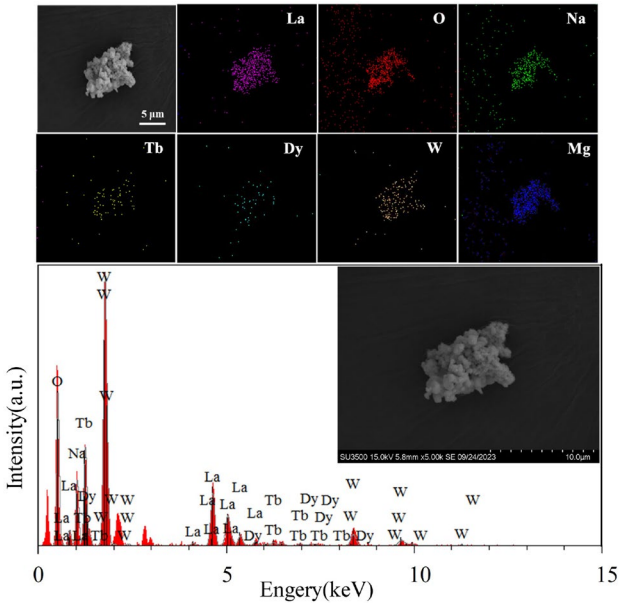

Fig. 4 SEM images, EDS spectrum and elemental mapping of NaLa0.84MgWO6: 0.08Dy^{3+}, 0.0.08Tb^{3+} phosphors

NLMWO: Dy^{3+} new yellow-emitting phosphors, as a yellow-emitting material with potential applications. However, no reports exist on the luminescent characteristics and the transmission mechanism for energy between Dy^{3+} and Tb^{3+} in NLMWO: Dy^{3+}, Tb^{3+} phosphors. In order to further investigate the luminescence behavior and mutual influence of Dy^{3+} and Tb^{3+} ions in the NLMWO substrate and to achieve energy transfer and tunable emissions, NLMWO: Dy^{3+}, Tb^{3+} phosphors were prepared and the experimental results were analyzed in this article.

In this work, a high-temperature solid-state method is used to generate a variety of NLMWO phosphors that are co-doped with Dy^{3+} and Tb^{3+}. The produced materials' morphology, luminous characteristics, and energy transfer mechanism were examined. Under the excitation of 389 nm wavelength, it was discovered that the NLMWO: Dy^{3+}, Tb^{3+} phosphors may switch between yellow and green emission by altering the ratio of Dy^{3+} and Tb^{3+}, while there was energy transfer in the NLMWO system. It has been demonstrated by the findings that the green NLMWO: Dy^{3+}, Tb^{3+} phosphor exhibits remarkable photoluminescent characteristics, suggesting it could be a feasible option as a material for w-LEDs.

2 Experiment

An array of $NaLa_{1-x}MgWO_6$:xDy^{3+}(x = 0.0–12 mol%), $NaLa_{1-y}MgWO_6$:yTb^{3+}(y = 0.0–12 mol%), $NaLa_{0.92-y}MgWO_6$:0.08Dy^{3+}, yTb^{3+}(y = 0.0–12 mol%) were effectively synthesized by high temperature solid phase technique. The components, Na_2CO_3 (99.8%), La_2O_3 (99.99%), Dy_2O_3 > (99.99%), $(MgCO_3)_4{\cdot}Mg(OH)_2{\cdot}5H_2O$ (99.99%), Tb_4O_7 > (99.99%), and WO_3 (99.8%), were precisely ground in an agate mortar after being weighed by stoichiometry. Grinded for half an hour and dried for 30 min in an 80 °C drying oven in an Al_2O_3 crucible. To characterize the sample, first, the muffle furnace was used to heat the dry powder. The powder was heated for 6 h at 900 °C and then further heated for 18 h at 1050 °C. The sample was heated and then cooled in the furnace until it reached room temperature. Next, to carry out the characterization, the burned samples were once more crushed to a powder.

Using an X-ray diffractometer (XRD-6100, Japan), the X-ray diffraction (XRD) patterns of the phosphors were captured using Cu Kα (λ = 0.154056 nm) radiation at 30 kV and 30 mA. The patterns were all gathered in a scanning mode with a step size of 0.01° for the 10–80° 2θ range. Use a scanning electron microscope (SEM-SU3500), the morphology was examined.

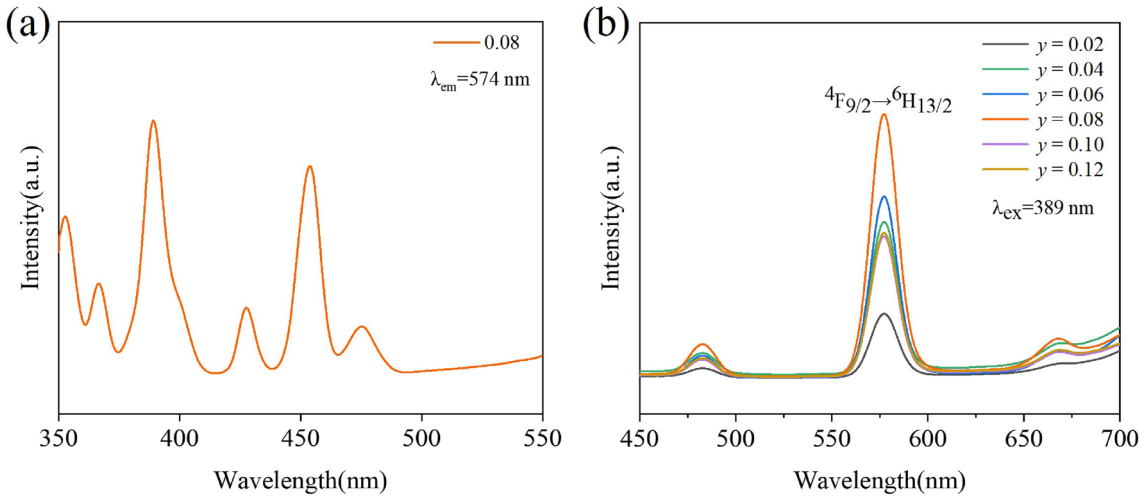

Fig. 5 **a** Excitation of NLMWO:xDy^{3+} phosphors; **b** emission spectra of NLMWO: xDy^{3+} phosphors

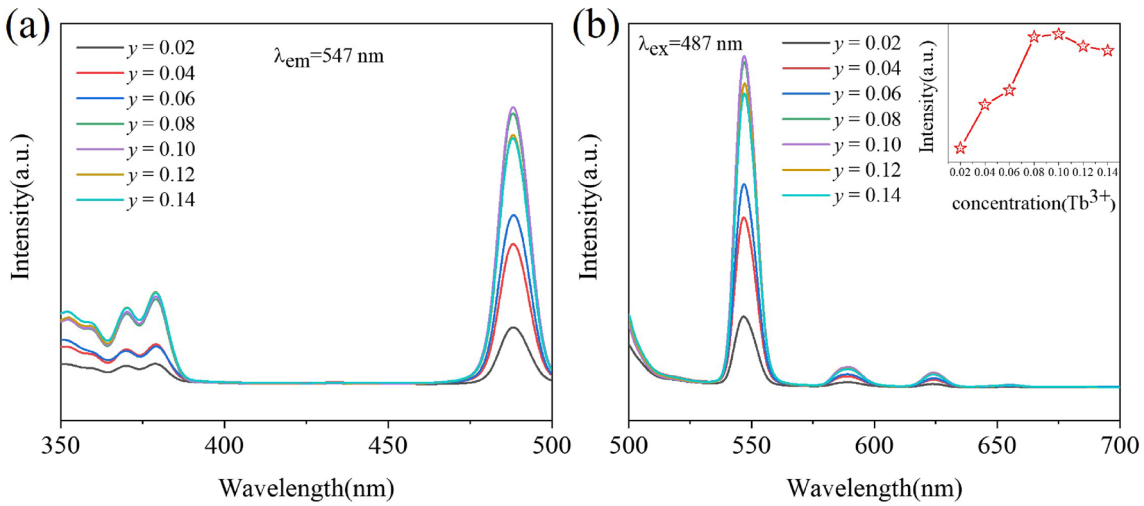

Fig. 6 **a** Excitation spectra of NLMWO:yTb^{3+} phosphors; **b** emission spectra of NLMWO: yTb^{3+} phosphors

An F-7000 fluorescence spectrophotometer was used to evaluate the materials' luminescence spectra at the temperature of the room.

3 Results and discussion

3.1 Crystal structure

$NaLa_{0.92-y}MgWO_6$:0.08Dy^{3+}, yTb^{3+}(y = 0.02, 0.04, 0.06, 0.08, 0.10, 0.12) series phosphors' XRD patterns are shown in Fig. 1. The sample's diffraction peaks match those on the reference card (JCPDF No. 37-0243) for the monoclinic double chalcogenide structure NLMWO, and there are no other impurity phases. It demonstrates that Dy^{3+} and Tb^{3+} were effectively incorporated into the host lattice without changing the structure of the crystals, and all the phosphors have a monoclinic double chalcogenide structure. Figure 1b shows that when rare earth ions are added, the angle of the diffraction peaks increases, according to the Bragg equation $2d\sin\theta = n\lambda$, the doping of Dy^{3+} and Tb^{3+} results in a lower lattice parameter and a bigger diffraction angle since the ionic radius of La^{3+} (1.032 Å) is larger than that of Dy^{3+} (0.912 Å) and Tb^{3+} (0.923 Å) [28].

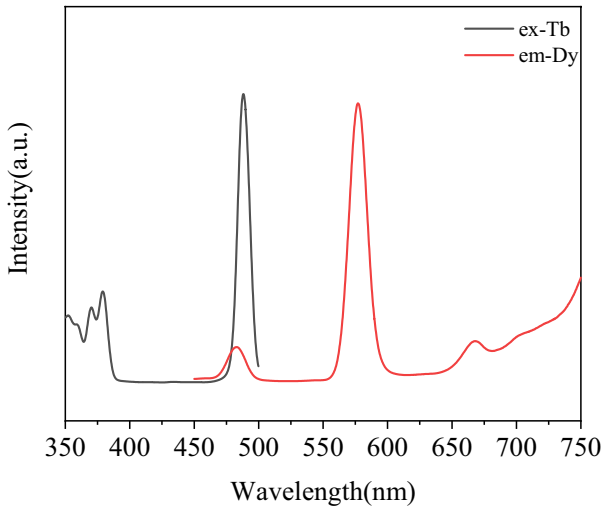

Fig. 7 Excitation of Tb^{3+} and the emission spectra of Dy^{3+}

Figure 2 shows the Rietveld refined pattern of $NaLa_{0.84}MgWO_6$: $0.08Dy^{3+}$, $0.08Tb^{3+}$. The starting model of this sample was taken from space group C2/m, and the refinement results obtained a low R convergence factor, where Rwp = 11.34% and Rp = 8.01%. These values are lower than 15%, indicating that the refinement results are reliable and good single-phase $NaLa_{0.84}MgWO_6$: $0.08Dy^{3+}$, $0.08Tb^{3+}$ phosphors are obtained, and their space group is C2/m.

Figure 3 shows the Raman spectra of NLMWO and $NaLa_{0.84}MgWO_6$: $0.08Dy^{3+}$, $0.08Tb^{3+}$. The shifts of the peaks observed in the range of 100 cm^{-1}–250 cm^{-1} are attributed to the correlation vibrations generated by the A-site cation and the ligand oxygen atoms. The peaks in the ranges of 360–390 cm^{-1} are attributed to the asymmetric deformation mode. The vibrations at around 800–900 cm^{-1} correspond to the short-range correlation of the atoms, and the shift of the peaks at that location may correspond to the oxygen octahedral symmetric stretching mode, which has less effect on the radius [29]. The shift of the peaks in Raman spectra also proves that the rare earth ions are successfully doped in.

3.2 Morphological study

Figure 4 shows the SEM patterns, EDS spectrum and elemental mapping of the samples, which shows that the particle sizes of the samples are between 1 and 2 μm, with irregular shapes, well-defined boundaries, and high crystallinity. The doping of ions has no significant effect on the crystal structure of NLMWO. EDS spectrum shows that Na, La, Mg, W, O, Dy and Tb ions are all present in the sample. The doped Dy and Tb ions completely enter the $NaLaMgWO_6$ host lattice. The elemental mapping demonstrates unequivocally that the elements are equally distributed throughout the co-doped phosphors for Dy^{3+} and Tb^{3+}.

3.3 Photoluminescence properties

The excitation spectrum of $NaLa_{0.92}MgWO_6$:$0.08Dy^{3+}$, measured at a wavelength of 547 nm, is shown in Fig. 5a. There are two strong peaks and four weak

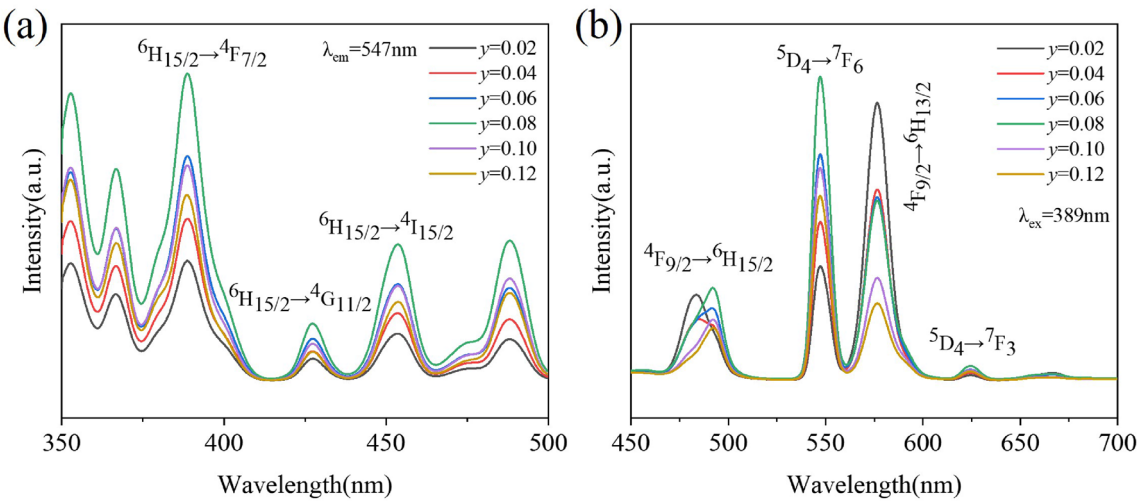

Fig. 8 **a** Excitation spectra of NLMWO:$0.08Dy^{3+}$; yTb^{3+} phosphors, **b** emission spectra of NLMWO:$0.08Dy^{3+}$, yTb^{3+}phosphors

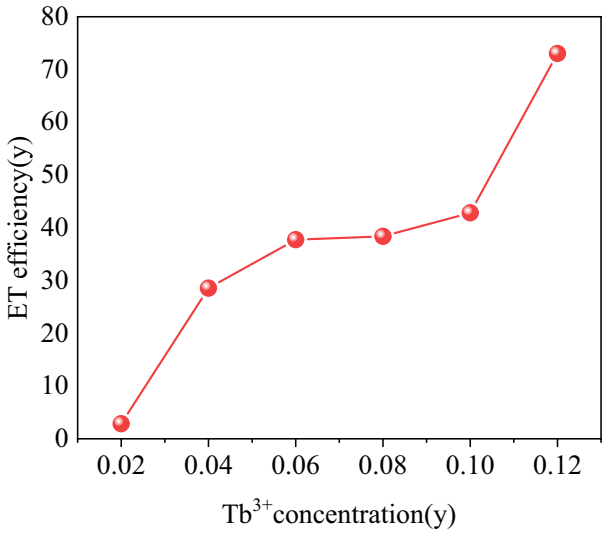

Fig. 9 Energy transfer efficiency between Dy^{3+} and Tb^{3+}in NaLa0.92-yDy0.08TbyMgWO6

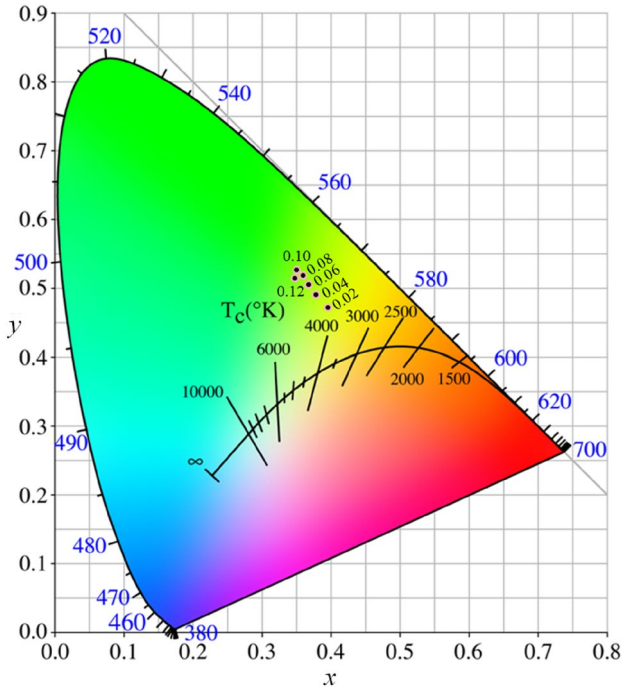

Fig. 10 CIE chromaticity diagram of NLMWO: $0.08Dy^{3+}$, yTb^{3+} phosphors

peaks in 350 – 550 nm, and the strong peak at 389 nm corresponds to $^6H_{15/2} \rightarrow {}^4F_{7/2}$ of Dy^{3+} transition. The spectrum emitted by $NaLa_{1-x}MgWO_6{:}xDy^{3+}$ when excited at a wavelength of 389 nm is presented in Fig. 5b. The $^4F_{9/2} \rightarrow {}^6H_{15/2}$ and $^4F_{9/2} \rightarrow {}^6H_{13/2}$ transitions of Dy^{3+} ions, which are responsible for the weak emission at 482 nm and the strong emission at 574 nm, respectively, are seen in this spectrum. At the same time, the data indicates that as the increases of Dy^{3+} concentration, the emission intensity shows a gradual rise and peaks at $x = 0.08$. After which, the concentration quenching causes a drop in intensity, therefore, it is inferred that the optimal doping amount of Dy^{3+} is 8% mol. The concentration burst is thought to be triggered by various interactions, including exchange interaction, multipole-multipole interaction, and radiation reabsorption. To identify the type of interaction that leads to concentration burst, one can calculate the critical distance (Rc) between Dy^{3+} ions using the Blasse formula [30]:

$$R_c = 2\left[\frac{3V}{4\pi X_c Z}\right]^{1/3} \quad (1)$$

where Z is the total amount of cations in the unit cell, V is the volume of the unit cell, and X_c is the quenching concentration. For NLMWO, $Z = 4$, $X_c = 0.08$, $V = 482.67$ Å^3. According to the formula, $R_c = 7.11$ Å, which is larger than 5 Å, demonstrating that the electric multipolar interaction is what causes the concentration quenching [31].

The $NaLa_{1-y}MgWO_6{:}yTb^{3+}$ excitation and emission spectra are shown in Fig. 6a and b, respectively. The excitation spectrum has several weak broadband peaks in the 350–400 nm and strong narrow peaks in the 470–500 nm wavelength ranges. Two faint peaks are seen at 370 and 379 nm, which correspond to the Tb^{3+} ions' transitions from the $^7F_6 \rightarrow {}^5L_{10}$ and $^7F_6 \rightarrow {}^5D_3$ energy levels, respectively. Additionally, there is a strong peak observed at 487 nm which corresponds to the transition of the Tb^{3+} ion from the $^7F_6 \rightarrow {}^5D_4$ energy level. Under excitation at a wavelength of 487 nm, Tb^{3+} ions have three characteristic emission peaks, which are caused by the $^5D_4 \rightarrow {}^7F_5$ (547 nm), $^5D_4 \rightarrow {}^7F_4$ (590 nm), $^5D_4 \rightarrow {}^7F_3$ (623 nm) transitions. The luminous intensity of $NaLa_{1-y}MgWO_6{:}yTb^{3+}$ is related to the Tb^{3+} ions doping concentration. As Tb^{3+} ion doping increases, the luminous intensity of phosphors initially rises and reaches its peak at $y = 0.10$. However, a downward trend is observed thereafter due to concentration quenching.

The excitation spectra of NLMWO:$0.10Tb^{3+}$ and the emission spectrum of NLMWO:$0.08Dy^{3+}$ are shown in Fig. 7. There exists a slight overlap in spectral range

Table 1 CIE coordinates of NLMWO: 0.08Dy^{3+}, yTb^{3+} phosphors

Tb^{3+}concentration	Sample compositions	CIE coordinates (*x*, *y*)
$y=0.02$	NLMWO:0.08Dy^{3+}, 0.02Tb^{3+}	(0.3960, 0.4719)
$y=0.04$	NLMWO:0.08Dy^{3+}, 0.02Tb^{3+}	(0.3790, 0.4903)
$y=0.06$	NLMWO:0.08Dy^{3+}, 0.02Tb^{3+}	(0.3685, 0.5049)
$y=0.08$	NLMWO:0.08Dy^{3+}, 0.02Tb^{3+}	(0.3596, 0.5192)
$y=0.10$	NLMWO:0.08Dy^{3+}, 0.02Tb^{3+}	(0.3513, 0.5267)
$y=0.12$	NLMWO:0.08Dy^{3+}, 0.02Tb^{3+}	(0.3483, 0.5143)

between 450 and 500 nm that is observable. The overlapping part includes the $^4F_{9/2} \rightarrow {}^6H_{15/2}$ transition of Dy^{3+} at 482 nm and the $^7F_6 \rightarrow {}^5D_4$ transition of Tb^{3+} at 487 nm. According to Dexter theory, an energy transfer can occur from Dy^{3+} to Tb^{3+}, where Dy^{3+} functions as a sensitizer by transferring energy to Tb^{3+}. This process enhances the luminescence intensity of Tb^{3+}. As a result, Dy^{3+} and Tb^{3+} co-doping was performed in NLMWO, and the energy transfer mechanism of Dy^{3+} and Tb^{3+} in NLMWO was investigated. The Dy^{3+} content was set at 0.08 and the Tb^{3+} doping quantity was varied.

The excitation and emission spectra of $NaLa_{0.92-y}MgWO_6$:0.08Dy^{3+}, yTb^{3+} are shown in Fig. 8. In Fig. 8a, the excitation spectra observed at the emission wavelength of 547 nm are monitored with both Dy^{3+} excitation peaks and Tb^{3+} ion excitation peaks, and the peak intensity at 389 nm is greater than the peak intensity at 487 nm. Under 389 nm excitation, the emission spectra of $NaLa_{0.92-y}MgWO_6$:0.08Dy^{3+}, yTb^{3+} sample are illustrated in Fig. 8b. The intensity of the Tb^{3+} characteristic emission peak first rises with the increase in Tb^{3+} concentration, reaches its maximum at $y = 0.08$, then the intensity gradually decreases. Tb^{3+} concentrations rise, which leads to a steady decline in the intensity of Dy^{3+} emission. This is because as the concentration of Dy^{3+} and Tb^{3+} ions increase, the concentration of activated ions increases, the interaction between Dy^{3+} and Tb^{3+} ions increase, the non-radiative transition increases, Dy^{3+} transfers energy to Tb^{3+} ions, and the luminescence intensity continues to decrease. Tb^{3+} ion concentration It first increases and then decreases. In addition to concentration quenching, the reason for the decrease is that defects caused by the oxygen gap will also capture part of the energy and cause the concentration to decrease [32, 33], none of the energy delivered by Dy^{3+} can make up for these losses. At the same time, yellow-green tunable emission is achieved by changing the ratio of Tb^{3+}/Dy^{3+} ion concentration. The following formula may be used to calculate the energy transfer efficiency [34]:

$$\eta_T = 1 - \frac{I_s}{I_{s0}} \quad (2)$$

where I_s and I_{s0} denote the intensity of Dy^{3+} in addition to or without Tb^{3+} doping, respectively. The computed value of η_T is shown in Fig. 9. The energy transfer efficiency grows linearly, as can be observed. When the doping amount is 0.12, the conversion capacity is as high as 73%. Its CIE coordinates are shown in the Fig. 10 and Table 1. One can observe that $NaLa_{0.90}MgWO_6$:0.08Dy^{3+},0.02Tb^{3+} emits a yellow color. As the concentration of Tb^{3+} rises, the phosphors' emission color shifts from yellow to green. At the same time, it can be seen that its correlated color temperature is low, located near 3000 k, and is suitable for optoelectronic devices and solid-state lighting [35] .

4 Conclusion

To sum up, a set of phosphors containing NLMWO: xDy^{3+}, yTb^{3+} were produced through solid-phase synthesis at high temperature. XRD results showed that the samples were successfully prepared without impurity phases. SEM and EDS results show that the preparation of the sample is uniform. In the NLMWO: xDy^{3+} phosphors, the best concentration of Dy^{3+} is 0.08 mol, the concentration burst is due to multipolar interactions. Photoluminescence results show that energy is transferred from Dy^{3+} to Tb^{3+}, and the conversion efficiency can be as high as 73%. The luminescent color of phosphors under UV stimulation shifts from yellow to green when the Tb^{3+} to Dy^{3+} ratio increases, realizing the yellow-green tunable emission, and the corresponding CIE coordinate changes from (0.3960, 0.4719) to (0.3483, 0.5143), indicating its potential application in w-LEDs.

Author contributions

ZW: prepared samples, characterized and writing-original draft; SZ: writing-original draft; PH, and ZH: provided Advice and financial support; ZZ: supervision, writing—review & editing. All authors read and approved the final manuscript.

Funding

This work was supported by the National Natural Science Foundation of China (Grant No. 52002293), the Startup Fund (Grant No. 22QD28) and Graduated Innovative Fund of Wuhan Institute of Technology (Grant No. CX2022229) for supporting this work.

Data availability

All data generated or analyzed during this study are included in this published article.

Declarations

Competing interests The authors declare that they have no known competing financial interests or personal relationships that could have appeared to influence the work reported in this paper.

Informed consent Informed consent was obtained from all individual participants included in the study.

Research involving human and animal participants This article does not contain any studies with human participants or animals performed by any of the authors.

References

1. G. Li, Y. Tian, Y. Zhao, J. Lin, Recent progress in luminescence tuning of Ce^{3+} and Eu^{2+}-activated phosphors for pc-WLEDs. Chem. Soc. Rev. **44**, 8688–8713 (2015). https://doi.org/10.1039/C4CS00446A
2. G. Blasse, Energy transfer between inequivalent Eu^{2+} ions. J. Solid State Chem. **62**, 207–211 (1986). https://doi.org/10.1016/0022-4596(86)90233-1
3. R.M. Pallares, X. Su, S.H. Lim, N.T.K. Thanh, Mn^{2+} and Mn^{4+} red phosphors: synthesis, luminescence and applications in WLEDs. a review. J. Mater. Chem. C. **4**, 53–61 (2016). https://doi.org/10.1039/C5TC02426A
4. J. Zhou, N. Sun, Z. Qiu, X. Huang, X. Wang, W. Zhang, Effect of Li^{+}, La^{3+} co-doping on the photoluminescence enhancement of $Sr_3AlO_4F:Sm^{3+}$ orange-red-emitting phosphor for white light-emitting diodes. Mater. Today. Commun. **29**, 102806 (2021). https://doi.org/10.1016/j.mtcomm.2021.102806
5. J. Liu, Z. Long, S. Xiao, X. Yang, K0.5La0.5SrMgWO6: Mn4+: a high-efficiency perovskite structure phosphor for plant cultivation LEDs. Mater. Today Commun. **31**, 103214 (2022). https://doi.org/10.1016/j.mtcomm.2022.103214
6. H.-R. Chen, C. Cai, Z.-W. Zhang, L. Zhang, H.-P. Lu, X. Xu, H. Van Bui, K.-H. Qiu, L.-J. Yin, Enhancing the luminescent efficiency of $Y_3Al_5O_{12}:Ce^{3+}$ by coating graphitic carbon nitride: toward white light-emitting diodes. J. Alloy. Compd. **801**, 10–18 (2019). https://doi.org/10.1016/j.jallcom.2019.06.122
7. J. Qiao, L. Ning, M.S. Molokeev, Y.-C. Chuang, Q. Liu, Z. Xia, Eu^{2+} site preferences in the mixed cation $K_2BaCa(PO_4)_2$ and thermally stable luminescence. J. Am. Chem. Soc. **140**, 9730–9736 (2018). https://doi.org/10.1021/jacs.8b06021
8. M.B. Gray, S. Hariyani, T.A. Strom, J.D. Majher, J. Brgoch, P.M. Woodward, High-efficiency blue photoluminescence in the $Cs_2NaInCl_6:Sb^{3+}$ double perovskite phosphor. J. Mater. Chem. C. **8**, 6797–6803 (2020). https://doi.org/10.1039/D0TC01037E
9. I. Gupta, S. Singh, S. Bhagwan, D. Singh, Rare earth (RE) doped phosphors and their emerging applications: a review. Cream. Int. **47**, 19282–19303 (2021). https://doi.org/10.1016/j.ceramint.2021.03.308
10. D. Tahaoğlu, H. Usta, F. Alkan, Revisiting the role of charge transfer in the emission properties of carborane-fluorophore systems: a TDDFT investigation. J. Phys. Chem. A **126**, 4199–4210 (2022). https://doi.org/10.1021/acs.jpca.2c02435
11. P. Halappa, H.M. Rajashekar, C. Shivakumara, Synthesis and structural characterization of orange red light emitting Sm^{3+} activated BiOCl phosphor for WLEDs applications. J. Alloy. Compd. **785**, 169–177 (2019). https://doi.org/10.1016/j.jallcom.2019.01.155
12. P. Halappa, A. Mathur, M.-H. Delville, C. Shivakumara, Alkali metal ion co-doped Eu^{3+} activated $GdPO_4$ phosphors: structure and photoluminescence properties. J. Alloy. Compd. **740**, 1086–1098 (2018). https://doi.org/10.1016/j.jallcom.2018.01.087

13. H. Liu, Z. Guo, Ce^{3+} and Dy^{3+} doped $Sr_3B_2O_6$: solid state synthesis and tunable luminescence. J. Lumin. **187**, 181–185 (2017). https://doi.org/10.1016/j.jlumin.2017.03.008
14. Y. Yang, X. Wang, B. Liu, Y. Zhang, X. Lv, J. Li, L. Wei, H. Yu, Y. Hu, H. Zhang, Molten salt synthesis and luminescence of Dy^{3+}-doped $Y_3Al_5O_{12}$ phosphors. Luminescence **35**, 580–585 (2020). https://doi.org/10.1002/bio.3759
15. B. Han, Y. Dai, J. Zhang, H. Shi, Luminescence properties of a novel yellow-emitting phosphor $NaLaMgWO_6$: Dy^{3+}. Mater. Lett. **204**, 145–148 (2017). https://doi.org/10.1016/j.matlet.2017.06.036
16. B. Devakumar, P. Halappa, C. Shivakumara, Dy^{3+}/Eu^{3+} co-doped $CsGd(MoO_4)_2$ phosphor with tunable photoluminescence properties for near-UV WLEDs applications. Dyes Pigm. **137**, 244–255 (2017). https://doi.org/10.1016/j.dyepig.2016.10.016
17. W. Costa Macedo, A. Germano Bispo Junior, K. De Oliveira Rocha, A.E. De Souza Albas, A.M. Pires, S. Rainho Teixeira, E. Longo, Photoluminescence of Eu^{3+}-doped CaZrO red-emitting phosphors synthesized via microwave-assisted hydrothermal method. Mater. Today Commun. **24**, 100966 (2020). https://doi.org/10.1016/j.mtcomm.2020.100966
18. X. Li, X. Gao, X. Zhang, X. Shen, M. Lu, J. Wu, Z. Shi, V.L. Colvin, J. Hu, X. Bai, W.W. Yu, Y. Zhang, Lead-free halide perovskites for light emission: recent advances and perspectives. Adv. Sci. **8**, 2003334 (2021). https://doi.org/10.1002/advs.202003334
19. X. Zhou, J. Qiao, Z. Xia, Learning from mineral structures toward new luminescence materials for light-emitting diode applications. Chem. Mater. **33**, 1083–1098 (2021). https://doi.org/10.1021/acs.chemmater.1c00032
20. J. Hou, X. Yin, F. Huang, W. Jiang, Synthesis and photoluminescence properties of $NaLaMgWO_6$:RE^{3+} (RE=Eu, Sm, Tb) phosphor for white LED application. Mater. Res. Bull. **47**, 1295–1300 (2012). https://doi.org/10.1016/j.materresbull.2012.03.023
21. G. Li, Y. Wang, Y. Wei, X. Wang, Structure, energy transfer, and luminescence properties of $NaLaMgWO_6$: Tb^{3+}, Eu^{3+} phosphors for solid-state lighting. J. Mater. Sci. Mater. Electron. **31**, 3835–3844 (2020). https://doi.org/10.1007/s10854-020-02918-6
22. T.-Y. Hwang, Y. Choi, Y. Song, N.S.A. Eom, S. Kim, H.-B. Cho, N.V. Myung, Y.-H. Choa, Fast synthesis of Dy^{3+} and Tm^{3+} co-doped double perovskite $NaLaMgWO_6$: a thermally stable singlephase white-emitting phosphor for WLEDs. J. Mater. Chem. C. **6**, 972–979 (2018). https://doi.org/10.1039/C7TC03576D
23. Y. Wu, F. Yang, F. Yan, R. Zuo, Tunable yellow–red emission performance of Dy^{3+}, Mn^{4+}: $NaLaMgWO_6$ phosphors excited with 390-nm LED. Appl. Phys. A **127**, 238 (2021). https://doi.org/10.1007/s00339-021-04392-1
24. S. García-Martín, E. Urones-Garrote, M.C. Knapp, G. King, P.M. Woodward, Transmission electron microscopy studies of NaLaMgWO6: spontaneous formation of compositionally modulated stripes. J. Am. Chem. Soc. **130**, 15028–15037 (2008). https://doi.org/10.1021/ja802511d
25. J. Zhang, Y. Dai, B. Liu, B. Han, Luminescence quenching of Er^{3+}/Sm^{3+} in color-tunable $NaLaMgWO_6$:Er^{3+}, Sm^{3+} phosphor. Optik **172**, 1129–1133 (2018). https://doi.org/10.1016/j.ijleo.2018.07.120
26. Y. Peng, Y. Huang, Z. Lei, H. Wang, J. Liu, Y. Mou, M. Chen, Rapid and efficient preparation of phosphor-in-glass converter by induction heating for high-power white LEDs/LDs. Mater. Today Commun. **29**, 102839 (2021). https://doi.org/10.1016/j.mtcomm.2021.102839
27. Q. Liu, X. Li, B. Zhang, L. Wang, Q. Zhang, L. Zhang, Structure evolution and delayed quenching of the double perovskite $NaLaMgWO_6$:Eu^{3+} phosphor for white LEDs. Ceram. Int. **42**, 15294–15300 (2016). https://doi.org/10.1016/j.ceramint.2016.06.169
28. R. Chen, X. Jiang, T. Zhang, Z. Leng, W. Yang, C. Li, H. Liu, C. Li, S. Li, L. Liu, H. Lin, F. Zeng, Z. Su, Study on energy transfer mechanism and optical properties of $LiLaSiO_4$: Dy^{3+}, Tb^{3+} phosphors with excellent thermal stability and color tunability. J. Lumin. **251**, 119168 (2022). https://doi.org/10.1016/j.jlumin.2022.119168
29. S. Wu, P. Xiong, Q. Liu, Y. Xiao, Y. Sun, E. Song, Y. Chen, Self-activated tungstate phosphor for near-infrared light-emitting diodes. Adv. Opt. Mater. (2022). https://doi.org/10.1002/adom.202201718
30. S.N. Ogugua, S.K.K. Shaat, H.C. Swart, O.M. Ntwaeaborwa, The influence of Dy^{3+} ions concentration and annealing on the properties of $LaGdSiO_5$:Dy^{3+} nanophosphors. J. Lumin. **179**, 154–164 (2016). https://doi.org/10.1016/j.jlumin.2016.06.056
31. Q. Ni, J. Huo, J. Liu, H. Yan, Q. Zhu, J. Li, C. Long, Q. Wang, Efficient $Ce^{3+} \rightarrow Tb^{3+}$ energy transfer pairs with thermal stability and internal quantum efficiency close to unity. Inorg. Chem. Front. (2022). https://doi.org/10.1039/D2QI01967A
32. K. Punia, G. Lal, S.K. Barbar, S.N. Dolia, P.A. Alvi, S. Dalela, S. Kumar, Oxygen vacancies mediated cooperative magnetism in ZnO nanocrystals: a d^0 ferromagnetic case study. Vacuum **184**, 109921 (2021). https://doi.org/10.1016/j.vacuum.2020.109921
33. K. Punia, G. Lal, P.A. Alvi, S.N. Dolia, S. Dalela, K.B. Modi, S. Kumar, A comparative study on the influence of monovalent, divalent and trivalent doping on the structural,

optical and photoluminescence properties of $Zn_{0.96}T_{0.04}O$ (T: Li^{+}, Ca^{2+}& Gd^{3+}) nanoparticles. Ceram. Int. **45**, 13472–13483 (2019). https://doi.org/10.1016/j.ceramint.2019.04.048

34. Y. Hua, J.S. Yu, Warm white emission of $LaSr_2F_7$:Dy^{3+}/Eu^{3+} NPs with excellent thermal stability for indoor illumination. J. Mater. Sci. Technol. **54**, 230–239 (2020). https://doi.org/10.1016/j.jmst.2020.02.066
35. A. Mathur, P. Halappa, C. Shivakumara, Synthesis and characterization of Sm^{3+} activated $La_{1-x}Gd_xPO_4$ phosphors for white LEDs applications. J. Mater. Sci. Mater. Electron. **29**, 19951–19964 (2018). https://doi.org/10.1007/s10854-018-0125-7